HHS Public Access

Author manuscript

J Med Chem. Author manuscript; available in PMC 2017 May 26.

Published in final edited form as:

J Med Chem. 2016 May 26; 59(10): 5102–5108. doi:10.1021/acs.jmedchem.6b00182.

Synthesis and Biological Evaluation of Vitamin D3 Metabolite 20*S*,23*S*-Dihydroxyvitamin D3 and Its 23*R* Epimer

Zongtao Lin[†], **Srinivasa R. Marepally**[†], **Dejian Ma**[†], **Tae-Kang Kim**[‡], **Allen SW. Oak**[‡], **Linda K. Myers**[§], **Robert C. Tuckey**[‖], **Andrzej T. Slominski**[‡,⊥], **Duane D. Miller**[†], and **Wei Li**[*,†]

[†]Department of Pharmaceutical Sciences, University of Tennessee Health Science Center, 881 Madison Avenue, Room 561, Memphis, Tennessee 38163, United States

[‡]Department of Dermatology, University of Alabama at Birmingham, Birmingham, Alabama 35294, United States

[§]Department of Medicine, University of Tennessee Health Science Center, Memphis, Tennessee 38163, United States

[‖]School of Chemistry and Biochemistry, University of Western Australia, Crawley, Western Australia 6009, Australia

[⊥]VA Medical Center at Birmingham, Birmingham, Alabama 35294, United States

Abstract

The vitamin D3 metabolite, 20*S*,23*S*-dihydroxyvitamin D3, was chemically synthesized for the first time and identified to be the same as the enzymatically produced metabolite. The C23 absolute configurations of both 20*S*,23*S*/*R*-dihydroxyvitamin D3 epimers were unambiguously assigned by NMR and Mosher ester analysis. Their kinetics of CYP27B1 metabolism were investigated during the production of their 1α-hydroxylated derivatives. Bioactivities of these products were compared in terms of vitamin D3 receptor activation, anti-inflammatory, and antiproliferative activities.

Graphical abstract

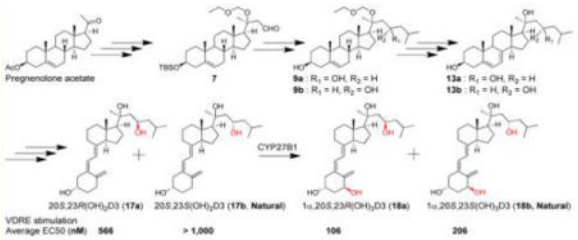

[*]**Corresponding Author:** Phone: 901-448-7532, Fax: 901-448-6828, wli@uthsc.edu.

Supporting Information

Preparation and characterization of compounds. The Supporting Information is available free of charge on the ACS Publications website at DOI: 10.1021/acs.jmedchem.6b00182. (PDF)

Notes

The authors declare no competing financial interest.

INTRODUCTION

The classical pathway for metabolism (Figure 1) of vitamin D3 (VD3) starts with hydroxylation at C25 by microsomal cytochrome P450 enzyme, CYP2R1,[1] or the mitochondrial CYP27A1,[2] producing 25-hydroxyvitamin D3 [25(OH)D3] primarily in the liver. 25(OH)D3 then undergoes 1α-hydroxylation in the kidney by CYP27B1, producing the active form of vitamin D3, 1α,25-dihydroxyvitamin D3 [1,25-$(OH)_2$D3]. Inactivation of 1,25$(OH)_2$D3 mainly involves CYP24A1-catalyzed hydroxylation and oxidation, ultimately producing calcitroic acid for excretion.[3,4]

An alternatively novel pathway of VD3 metabolism is initiated by CYP11A1.[5–8] CYP11A1 can metabolize VD3 into several mono-, di-, and trihydroxylated bioactive metabolites, with 20*S*-hydroxyvitamin D3 [20*S*(OH)D3] and 20*S*,23-dihydroxyvitamin D3 [20*S*,23$(OH)_2$D3] being the most comprehensively studied so far.[9] These two metabolites were initially produced enzymatically in vitro by incubating VD3 with bovine CYP11A1.[5,6] Subsequent investigations detected the formation of these metabolites from VD3 in keratinocytes, adrenal glands, and human placenta, indicating the occurrence of these CYP11A1-mediated pathways in these cells or tissues.[7–9] Final proof on the occurrence of this pathway in vivo was detection of 20*S*(OH)D3, 20*S*,23$(OH)_2$D3, and related hydroxy derivatives in the human epidermis and serum.[10] Interestingly, the epidermal levels of 20*S*(OH)D3 and 22(OH)D3 were higher than that of 25(OH)D3 but lower in the serum, however, at levels above those required for biological activity as measured in vitro.[10]

The biological activities of 20*S*(OH)D3 and 20*S*,23$(OH)_2$D3 have been demonstrated in a large number of in vitro and in vivo systems.[9,11,12] They are biased agonists of the vitamin D receptor (VDR) and share many but not all biological actions of 1,25$(OH)_2$D3.[9,11,12] Both of them are inverse agonists on RORα and RORγ.[13] They inhibited the proliferation and stimulated differentiation of epidermal keratinocytes and leukemia cells from human and mouse[14,15] and showed antimelanoma activity.[11,16] In addition, 20*S*(OH)D3 and 20*S*,23$(OH)_2$D3 exerted their anti-inflammatory activities through downregulation of NFκB activity in normal and immortalized keratinocytes[17–19] and displayed antifibrotic effects on human dermal fibroblasts from scleroderma patients and antifibrotic activity in animal models.[20] 1,25$(OH)_2$D3 is a strong inducer of CYP24A1 which catalyzes the inactivation of vitamin D metabolites,[21] whereas 20*S*(OH)D3 and 20*S*,23-$(OH)_2$D3 are poor stimulators of CYP24A1 expression, suggesting they are less prone to rapid metabolism by this enzyme.[9] Moreover, while 1,25$(OH)_2$D3 causes hypercalcemia in rats and mice, both 20*S*(OH)D3 and 20*S*,23$(OH)_2$D3 are noncalcemic at much higher doses (up to 30 μg/kg in mice).[15,22] Thus, 20*S*(OH)D3 and 20*S*,23$(OH)_2$D3 have great potential for further development as adjuvant therapeutic agents, especially for a wide variety of immune-driven diseases.

While the structure of enzymatically produced 20*S*,23-$(OH)_2$D3 has been elucidated by NMR analysis,[6] the absolute configuration at C23 has not been determined unambiguously due to the limited amount of material available. It is well-known that the absolute configuration of molecules can have substantial impacts on their biological activities. Therefore, the aim of this study was to (1) synthesize both epimers of 20*S*,23*R*/*S*$(OH)_2$D3 chemically and determine their absolute configurations by NMR and Mosher ester analyses;

(2) identify which epimer corresponds to the enzymatically generated, biologically active 20*S*,23(OH)$_2$D3 metabolite by using HPLC and NMR; (3) evaluate the ability of CYP27B1 to metabolize these two epimers for the production of their 1α-OH derivatives; and (4) assess the differential biological activities for these two epimers as well their 1α-OH derivatives with respect to VDR activation, antiproliferative and anti-inflammatory effects.

RESULTS AND DISCUSSION

Chemistry

The synthetic route to make 20*S*,23*R*(OH)$_2$D3 and 20*S*,23*S*(OH)$_2$D3 is shown in Scheme 1. Detailed synthesis procedures and structural characterizations of intermediates and products are listed in the Supporting Information (SI). Briefly, the 3-acetyl on commercially available pregnenolone acetate **(1)** was first replaced by TBS protection after deacetylation under basic condition.[23] This replacement allowed 3-OTBS to go through later Grignard reactions and hydroboration safely and intact. Addition of vinyl magnesium bromide to 20-ketone **(3)** afforded alcohol **4** with a stereospecific 20*S* configuration as reported in our previous studies.[21,24,25] The 20-OH was then protected by EOMCl and excess DIPEA in DCM with satisfactory yield (92%). Intermediate **6** was obtained by 9-BBN hydroboration and went through PDC oxidation to give aldehyde **7**, in which the aldehyde group was utilized to react with isobutylmagnesium bromide to produce two epimers (**8a** and **8b**) with different C23 configuration. Our initial trials to separate **8a** and **8b** using different solvent systems for normal phase TLC failed to obtain pure diastereomers. Fortunately, after being treated with TBAF, mixture **8** gave two separated spots (alcohols **9a** and **9b**) on TLC which were further separated using flash column chromatography for the following reactions. Diacetylation of 3-OH and 23-OH on **9** afforded protected **10**, which was subsequently transformed into the 5,7-diene 7DHC structure **(11)** by a well-established procedure using dibromantin/AIBN/TBAB/TBAF conditions.[26] EOM protection on C20 was removed to keep the configurations of 3-OH and 23-OH unaffected. In this study, montmorillonite K10 clay was found to be a neat catalyst for the removal of EOM protection at room temperature. Hydrolysis of ester bonds under KOH/MeOH condition rapidly yielded the 7DHC structure **(13)**. To get secosteroid structures, B-ring-opening reaction using UVB light irradiation was carried out for **13** dissolved in ethyl ether, followed by heat induced isomerization of previtamin D3 to produce VD3 product (**17a** as isomer I or **17b** as isomer II). Normal phase LC was unable to separate **17** out of the reaction mixture, so HPLC was used for the purification of **17** using acetonitrile (ACN) and water as mobile phases. 1α-Hydroxylated product **18** was produced by enzymatic reaction with CYP27B1, which is highly specific for the 1α-position based on its function,[27] and was purified by HPLC.

Isomer II (17b) Showed Matched Retention Times with the CYP11A1 Product in HPLC Chromatograms

To determine which one of the chemically synthesized 20*S*,23-(OH)$_2$D3 epimers is identical to the CYP11A1 product, HPLC analysis was carried out to compare their chromatographic behaviors. As shown in Figure 2, isomer II under different reverse phase HPLC conditions (methanol:water for A and B, and acetonitrile:water for C and D) gave the same retention

times as that of enzymatically produced 20*S*,23(OH)$_2$D3, strongly suggesting that isomer II has the same structure as the natural metabolite discovered previously.[6,14]

In addition, our previous study has elucidated the structure of enzymatic 20*S*,23(OH)$_2$D3, and the NMR and UV spectra of synthetic **17b** further confirmed that it was identical to the reported natural product. For comparison, the spectra of **17a** and **17b** are listed in SI (Figures S22–S30 for spectra and Table S2 for proton NMR chemical shift assignments). Highresolution MS spectra obtained using a Waters UPLC coupled to a Xevo G2-S qTof MS system also confirmed their identical structures using an optimized method.[28,29]

Identification of 9a Having a 23*R* Configuration and 9b Having a 23*S* Configuration by NMR

To determine the C23 configurations of isomer I **(17a)** and isomer II **(17b)**, intermediates **9a** and **9b** maintaining the same C23 configurations with **17a** and **17b** were used. Their NMR (1D and 2D) spectra were recorded and compared to assign their C23 configurations with assistance of molecular modeling. Their HSQC, HMBC, and NOESY spectra are shown in Figure 3 and SI Figures S1–S13. The assignments of their ^{1}H and ^{13}C chemical shifts are listed in SI Table S1. Six methyl signals belonging to the ring system (18-, 19-, 21-, 26-, and 27- methyls) and one from EOM protection, CH groups, and CH_2 groups were all identified on HSQC (SI Figure S11). All four quaternary carbons (C5, C10, C13, and C20) were assigned based on their HMBC spectra (SI Figure S12). The assignment strategy is similar to that of previously reported di- and trihydroxyvitamin D3 metabolites.[6,24]

Distances used to distinguish the two epimers are shown in Figure 3. NOE integrals of 6H to $7H_\beta$ and to $4H_\alpha$ were used as internal references to calibrate other NOE peak integrals (SI Figure S13). The NOE integrals of reference protons in **9a** and **9b** are comparable as seen in the middle panels of Figure 3B,C (or SI Figure S13); however, the NOE peak integral of 23H to the centroid of 21-CH_3 in **9a** (Figure 3B, left panel) is 2.5 times smaller than that in **9b** (Figure 3C, left panel). On the basis of the internal reference distances, the calculated distance between 23H and the centroid of 21-CH_3 in **9a** (3.94 Å) is larger than that in **9b** (2.98 Å) (Figure 3A). On the basis of the modeling structures incorporating these NOE distance constraints, we tentatively conclude that **9a** and **9b** have 23*R* and 23*S* configurations, respectively.

Further NMR evidence for the C23 stereochemistry of **9a** and **9b** is provided by the chemical shifts of neighboring C22 protons as shown in the right panels of Figure 3B,C. In the 23*R* (**9a**) modeled structure, 23-O and 20-O are oriented toward opposite directions, while they are oriented toward similar directions in the 23*S* (**9b**) configuration (Figure 3A). Consequently, the two germinal protons at C22 experience a relatively similar chemical environment in 23*R* (**9a**) and a very different chemical environment in 23*S* (**9b**). The related distances are shown in Figure 3A. The two C22 germinal protons showed a similar chemical shift (both are at 1.68 ppm) in **9a** but very different chemical shifts (1.92 and 1.58 ppm) in **9b** (SI Table S1). Therefore, the chemical shift patterns of the two protons in 22-CH_2 also suggest that the 23 configuration of **9a** is *R*, and **9b** is *S*.

Confirmation of the 23*R* Configuration of 9a by Mosher Ester Analysis

To confirm our tentative assignments that **9a** has a 23*R* configuration based on the above NMR analysis, we performed the Mosher ester analysis for **9a**. In this intermediate, there are two free OH groups, and two reactions were carried out by transforming **9a** to *S*- and *R*-Mosher 3,23-diesters, separately (Scheme 2). The 3-OH has a known β position which makes C3 an *S* configuration, 3*S* is thus used as an internal reference. The ^{1}H NMR, ^{1}H–^{1}H COSY, and ^{19}F-NMR spectra of *S*- and *R*-Mosher esters of **9a** are shown in SI Figure S14–S19. The ^{1}H chemical shifts of 2-CH_2 and 4-CH_2 were used to verify the 3*S* configuration, and the ^{1}H chemical shifts of 22-CH_2 and 24-CH_2 were used to determine the C23 configuration. The results of Mosher ester analysis are shown in Table 1. C23 of **9a** was unambiguously identified as 23*R* according to the chemical shifts of 22-CH_2 and 24-CH_2 in the *S*- and *R*-Mosher esters, **9b** was thus assigned as 23*S*. Because **17a** and **17b** were produced from **9a** and **9b** separately with intact C23 configurations, they were assigned as 20*S*,23*R*$(OH)_2$D3 and 20*S*,23*S*$(OH)_2$D3, respectively. This assignment is consistent with the NMR analyses described earlier.

Kinetics of the Metabolism of 20*S*,23*R*$(OH)_2$D3 (17a) and 20*S*,23*S*$(OH)_2$D3 (17b) by Mouse CYP27B1

CYP27B1 plays a key role in the activation of 25(OH)D3 to 1,25$(OH)_2$D3 and can also 1α-hydroxylate 20*S*,23$(OH)_2$D3 which alters its biological properties.[4,30,31] We therefore compared the abilities of mouse CYP27B1 to hydroxylate **17a** and **17b** (Table 2). CYP27B1 specifically adds a 1α-OH group to a range of VD3 analogues including 25(OH)D3, 20*S*(OH)D3,20*S*,24*R*$(OH)_2$D3,and 20*S*,24*S*$(OH)_2$D3.[4,24,27,30,31] Using well established procedures,[30,31] **17b** was converted to **18b** by CYP27B1, as further confirmed by using an authentic, enzymatically produced standard.[27] **17a** was presumably metabolized into its 1α-hydroxylated product based on the hydroxylation specificity of CYP27B1 for this position.[4,31] **17a** displayed both K_m and k_{cat} values half those for **17b**, therefore the overall catalytic efficiency (k_{cat}/K_m) of CYP27B1 for metabolism of these two epimers is approximately the same. However, the higher k_{cat} value for **17b** indicates that CYP27B1 has a higher capacity to hydroxylate this compound than its unnatural epimer having a 23*R*-configuration when substrate concentrations are high.

The Abilities of 20*S*,23*R*$(OH)_2$D3, 20*S*,23*S*$(OH)_2$D3 and Their 1α-OH Derivatives to Activate the VDR

The VDR is known to mediate many activities of vitamin D compounds and has been shown to be required for the stimulation of differentiation and CYP24A1 expression in keratinocytes by enzymatically produced **17b**.[18] To test the differential abilities of **17a** and **17b** together with their 1α-hydroxylated derivatives, to activate the VDR, a synthetic VDR transcriptional promoter (VDRE) was transduced into three different cell lines previously used for a lentiviral VDRE-luciferase reporter assay.[21,24] The three cell lines used were HaCaT cells as a model of normal human keratinocyte, Caco-2 cells as a cancer cell model, and Jurkat cells as an immune cell model. Two well-known VDR agonists, 1,25$(OH)_2$D3 and 22-oxa-1,25$(OH)_2$D3, were used as positive controls in this assay. Both of them showed low EC_{50} values for VDR activation using the luciferase reporter assay in all three cell lines

(Table 3), with 22-oxa- 1,25(OH)$_2$D3 being more potent than 1,25(OH)$_2$D3. In particular, they gave low nM EC$_{50}$s in Jurkat cells, suggesting their selectivity among different cell types. Importantly, **17b** was unable to activate VDR at a concentration up to 1000 nM, while **17a** showed a strong stimulatory effect at this concentration in all three cell lines, indicating that the 23*R* configuration favors VDR activation with the synthetic VDRE used, compared to the 23*S* epimer. Both 1α-OH derivatives (**18a** and **18b**) were more potent than their parent compounds, consistent with 1α-hydroxylation causing activation, as for 25(OH)D3.[4,27] Molecular modeling also suggests increased binding interactions of the 1α-OH derivatives (**18a** and **18b**) to the VDR than for **17a** and **17b** (SI Figure S32). Similarly, 18a with a 23*R* configuration showed a lower EC$_{50}$ value than **18b** with a 23*S* configuration, particularly in Jurkat cells, which is consistent with the relative potencies of **17a** and **17b** (parent compounds).

Upregulation of LAIR1 Levels As a Marker of AntiInflammatory Activity

Leukocyte-associated immunoglobulin-like receptor 1 (LAIR1), also called CD305 (cluster of differentiation 305), is an inhibitory receptor expressed in peripheral mononuclear cells including natural killer cells, T cells, and B cells in the immune system.[32] This inhibitory receptor downregulates immune responses and prevents cell lysis, thus it is recognized as an anti-inflammatory protein marker in autoimmunity.[32] Previously, we reported that 20*S*,24*S*/*R*(OH)$_2$D3 and their 1αOH derivatives upregulate the concentration of LAIR1, indicating their anti-inflammatory effects.[24] To test whether 20*S*,23*S*/*R*(OH)$_2$D3 and their 1αOH-derivatives also possess anti-inflammatory activities, we measured LAIR1 levels by flow cytometry in mice splenocytes following treatment with these secosteroids. Table 3 shows that all these compounds including the two positive controls significantly elevated the level of LAIR1 at a concentration of 100 nM. **17a**, **17b**, **18a**, and **18b** showed increases comparable with that of 22-oxa-1,25(OH)$_2$D3, and these effects were stronger than that of 1,25(OH)$_2$D3. In addition, **18a** and **18b** showed similar stimulatory effects to their parent compounds (**17a** and **17b**), indicating that 1α-hydroxylation is not necessary for the anti-inflammatory activity of these secosteroids. These finding are consistent with previously reported inhibitory effects of 20*S*(OH)D3 and 20*S*,23(OH)D3 on production of pro-inflammatory cytokines by mouse and human lymphocytes.[9,13]

Finally, we tested the antiproliferative activity of these compounds on SKMEL-188 melanoma cells (SI Figure S33). All D3 derivatives moderately inhibited growth of melanoma cells at concentrations of 0.1–1.0 nM in a dose-dependent manner, similar to the classical 1,25(OH)$_2$D3 (the effect was statistically significant). The IC$_{50}$ values ranged from 10^{-11} to 10^{-10} M, being similar for the 20,23(OH)$_2$D3 isomers, their 1αOH-derivatives (**18a** and **18b**) and 1,25(OH)$_2$D3. However, **18a** and **18b** showed higher maximal inhibition values (SI Figure S33), suggesting that addition of a 1αOH can potentiate the antiproliferative effect.

In this study, the bioactive VD3 metabolite 20*S*,23*S*(OH)$_2$D3 (**17b**) and its non-natural epimer 20*S*,23*R*(OH)$_2$D3 (**17a**) were chemically synthesized, and their C23 configurations were unambiguously assigned by NMR and Mosher ester analyses. **17b** was identified as the enzymatic product of VD3 metabolism by CYP11A1[6] by HPLC and NMR. Comparison of

the kinetics of **17a** and **17b** metabolism by CYP27B1 showed that they have similar catalytic efficiencies for 1α-hydroxylation. This enzymatic 1α-hydroxylation was exploited to make small quantities of **18a** and **18b** for analyzing the effect of the 1α-hydroxyl group on biological activity. Using a synthetic VDRE construct and a luciferase reporter assay, we observed that **17a**, but not **17b**, could cause VDR activation. The modest activation of the VDRE by **17a** is consistent with low activation of VDRE of CYP24A1 promoter in our previous study in keratinocytes and leukemia cells, where involvement of the VDR was demonstrated.[11,18] This is also consistent with our assessment that these compounds act as biased agonists on VDR signaling system[9,11,12] and that their biological activity also involves RORs.[13] Both epimers caused VDRE transcriptional activation following 1α-hydroxylation, with the 23*R* epimer being more potent. These results are consistent with our previous observations on the relative potencies of 20*S*,24*R*/*S*(OH)$_2$D3.[24] 23*R*- and 23*S*-epimers, 1α-hydroxylated or not, showed somewhat different potencies in all three cell lines tested, suggesting an enhanced interaction with the VDR/VDRE complex in immune cells, possibly due to high expression of the VDR or high concentrations of specific coactivators in immune cells that mediate the VDR responses, compared to the other cells tested.[4] Interestingly, the EC_{50} for **18a** in Jurkat cells was six times lower than that of **18b**. Analysis of the docking of these compounds using the VDR crystal structure further correlated their potencies to their binding interactions with the VDR, with 1α-hydroxylation markedly increasing the docking score. The anti-inflammatory potential of the C23 epimers was assessed by their ability to increase LAIR1 levels and their antiproliferative ability from the MTS assay, which measures mitochondrial activity. Results reveal that the C23 epimers, both with and without a 1α-hydroxyl group, have potent anti-inflammatory and antiproliferative activities, better or at least comparable with that of 1,25(OH)$_2$D3 and/or 22-oxa. The lack of a requirement for 1α-hydroxylation for the anti-inflammatory activity of the novel secosteroids is consistent with the recent discovery that they act as inverse agonists on RORγ, a driver of proinflammatory responses.[13] In contrast, addition of a 1α-OH group to the novel secosteroids can increase their affinity toward the VDR,[12] leading to improved antiproliferative activity.[9] The exact mechanisms and structural requirements for these different biological activities remain to be elucidated with further in-depth mechanistic studies.

CONCLUSION

In summary, 20*S*,23*R*/*S*(OH)$_2$D3 (**17a/17b**) and their 1α-OH metabolites (**18a/18b**) were synthesized for the first time, and 20*S*,23*S*(OH)$_2$D3 (**17b**) was confirmed to be the natural metabolite. These compounds showed different abilities to activate the VDR, with **18a** being the most potent. They all showed anti-inflammatory and antiproliferative activities, although these different biological activities were not linearly correlated, most likely due to distinct mechanisms and structural requirements leading to these biological activities. Further biological studies of the unnatural metabolite, **18a**, will be necessary to investigate its drug-like properties in comparison to its natural 23*S* counterpart.

EXPERIMENTAL SECTION

General Procedures

See SI for chemistry procedures of intermediates and final products.

HPLC

Purities (SI Figure S28–S29) of final VD3 products (**17a** and **17b**) were determined by using an Agilent HPLC 1100 system and a Phenomenex Luna-PFP C18 column (5 μm, 250 mm × 4.6 mm, Torrance, CA) at 25 °C and a flow rate of 1.0 mL/min. Acetonitrile and water were used as mobile phases with a gradient comprising 40–70% acetonitrile for 30 min; 263 nm was used to display chromatograms. The purities of **17a** and **17b** were determined as ≥98%.

For identifying which chemically synthesized product was identical to enzymatic product by HPLC, retention times of chemically synthesized isomer I (**17a**) and isomer II (**17b**) were compared with that of enzymatic 20*S*,23(OH)2D3. HPLC was carried out on a C18 column (Grace Alltima, 25 cm × 4.6 mm, 5 μm), with secosteroids being monitored by a UV detector at 265 nm. Two different solvent systems were used, 64–100% methanol for 20 min, then 100% methanol for 25 min or 45–100% acetonitrile for 25 min, then 100% acetonitrile for 25 min. The flow rate was 0.5 mL/min.

NMR

All NMR data were collected on a Bruker Avance III 400 MHz NMR (Bruker BioSpin, Billerica, MA). Samples were dissolved in 0.5 mL of $CDCl_3$, and NMR data were collected at room temperature. TMS was used as an internal standard.

Metabolism of the C23 Epimers by CYP27B1

To measure the kinetics of 17a and 17b metabolism by CYP27B1, substrate was incorporated into phospholipid (PL) vesicles at a range of concentrations (0.0025–0.07 mol/mol PL).[24,30,31] The amount of product after a 3 min incubation with 0.1 μM mouse CYP27B1 was determined by HPLC.[30] Kinetic parameters were determined by fitting the Michaelis–Menten equation to the data with Kaleidagaph 4.1.1. Data for K_m and K_{cat} are presented as mean ± standard error of the curve fit. This procedure was scaled up and the incubation time extended to 1 h to produce μg amounts of the 1α-hydroxy derivatives for biological testing, as described before.[30,31] After incubation, the product (**18a** or **18b**) was extracted with dichloromethane, dried, and purified by HPLC on a C18 column (Grace Alltima, 25 cm × 4.6 mm, 5 μm) using an acetonitrile in water gradient at a flow rate of 0.5 mL/min: 45–100% acetonitrile for 25 min then 100% acetonitrile for 25 min. The two epimers were further purified on the same column using a methanol gradient: 46–100% methanol for 15 min then 100% methanol for 25 min, at 0.5 mL/min.

Cell Cultures

HaCat, Caco-2, and Jurkat cells were transduced with a lentiviral VDRE-luciferase reporter vector as before.[21,24] Cells were grown in media as follows. Caco-2 cells: Dulbecco's Modified Eagle Medium (DMEM) supplemented with 10% fetal bovine serum (FBS) and 1% penicillin/streptomycin/amphotericin antibiotic solution (Ab) (Sigma-Aldrich, St. Louis,

MO). HaCaT cells: The same medium used for Caco-2 cells with 10% FBS changed into 5% FBS. Jurkat cells: RPMI 1640 medium supplemented with 10% FBS and 1% Ab. Splenocytes from mice: Eagles Minimal Essential Medium (EMEM) supplemented with 9% charcoal-stripped FBS, 100 U/mL penicillin, and 100 μg/mL streptomycin, nonessential amino acids, 2.5 mM 2-mercaptoethanol, and 2.5 mM L-glutamine. SKMEL-188 melanoma cells: Ham's F10 medium supplemented with 5% FBS and 1% Ab. All cells were cultured at 37 °C in a humidified atmosphere containing 5% CO_2.

VDRE-Luciferase Transcriptional Reporter Assay

HaCaT, Caco-2, and Jurkat cells were selected for 1 week by culturing in medium containing additional 1.0 μg/mL puromycin. Each cell line was then plated in a 96-well plate (10000 cells/well, 100 μL medium) using FBS-free media and incubated for 24 h to synchronize the cells. Secosteroids at a series of concentrations were added separately to 96-well plate (1.0 μL/well). The final concentration of DMSO was 0.1%. Cells were incubated for another 24 h, and then 100 μL of solution of ONE-Glo luciferase assay system (Promega, Madison, WI) was added to each well. After 5 min reaction at room temperature, the luciferase signal was detected by a BioTek Synergy HT microplate reader (BioTek Instruments, Inc., Winooski, VT, US). All concentrations of secosteroids were tested in triplicate.

Measurement of LAIR1 Concentrations by Flow Cytometry

Splenocytes isolated from DBA/1 mice were used to measure the LAIR1 levels. The cells were treated with each secosteroid at a concentration of 10^{-7} M, ethanol was used as vehicle control. After overnight incubation, cells were labeled with specific fluorochrome antibodies for both CD4 (BD Biosciences, San Jose, CA) and LAIR1 (eBioscience, San Diego, CA). The LAIR1 level was then determined by flow cytometry (multiparameter) using an LSRII flow cytometer (BD Biosciences, San Jose, CA) when gating was performed on CD4 cells. At least 10000 cells were analyzed from each sample. Final results were obtained from Flow software (Tree Star, Ashland, OR) analysis. Results are expressed as the mean of quadruplicate values ± standard error ($n = 4$).

Supplementary Material

Refer to Web version on PubMed Central for supplementary material.

Acknowledgments

This work was supported by NIH grants 1R21AR063242 (W.L., D.D.M.), 1S10OD010678 (W.L.), 1S10RR026377 (W.L.), 2R01AR052190 (AS.), 1R01AR056666-01A2 (AS.), and R21AR066505 (A.S.). The content is solely the responsibility of the authors and does not necessarily represent the official views of the NIH.

ABBREVIATIONS USED

1,25(OH)$_2$D3	1α,25-dihydroxyvitamin D3
20*S*(OH)D3	20*S*-hydroxyvitamin D3
20*S*,23(OH)$_2$D3	20*S*,23-dihydroxyvitamin D3

22-oxa	22-oxa-1α,25-dihydroxyvitamin D3
25(OH)D3	25-hydroxyvitamin D3
7DHC	7-dehydrocholesterol
9-BBN	9-borabicyclo[3.3.1]nonane
Ab	penicillin/streptomycin/amphotericin antibiotic solution
ACN	acetonitrile
AIBN	azobis(isobutyronitrile)
COSY	^{1}H–^{1}H correlation spectroscopy
CYP	cytochrome P450 enzyme
DIPEA	diisopropylethylamine
DMF	dimethylformamide
DMAP	4-dimethylaminopyridine
EOMCl	chloromethyl ethyl ether
HMBC	^{1}H–^{13}C heteronuclear multiple bond correlation spectroscopy
HSQC	^{1}H–^{13}C heteronuclear single quantum correlation spectroscopy
LAIR1	leukocyte-associated immunoglobulinlike receptor 1
PDC	pyridinium dichromate
TBAB	tetra-*n*-butylammonium bromide
TBAF	tetra-*n*-butylammonium fluoride
TBSCl	*tert*-butyldimethylsilyl chloride
TOCSY	^{1}H–^{1}H total correlation spectroscopy
VD3	vitamin D3
VDR	vitamin D receptor
VDRE	vitamin D response element

References

1. Zhu JG, Ochalek JT, Kaufmann M, Jones G, Deluca HF. CYP2R1 is a major but not exclusive contributor to 25-hydroxyvitamin D production in vivo. Proc Natl Acad Sci USA. 2013; 110:15650–15655. [PubMed: 24019477]

2. Haussier MR, Whitfield GK, Haussier CA, Hsieh JC, Thompson PD, Selznick SH, Dominguez CE, Jurutka PW. The nuclear vitamin D receptor: biological molecular regulatory properties revealed. J Bone Miner Res. 1998; 13:325–349. [PubMed: 9525333]

3. Tieu EW, Tang EK, Chen J, Li W, Nguyen MN, Janjetovic Z, Slominski A, Tuckey RC. Rat CYP24A1 acts on 20-hydroxyvitamin D(3) producing hydroxylated products with increased biological activity. Biochem Pharmacol. 2012; 84:1696–1704. [PubMed: 23041230]

4. Lin Z, Li W. The roles of vitamin D its analogs in inflammatory diseases. Curr Top Med Chem. 2016; 16:1242–1261. [PubMed: 26369816]

5. Slominski A, Semak I, Zjawiony J, Wortsman J, Li W, Szczesniewski A, Tuckey RC. The cytochrome P450scc system opens an alternate pathway of vitamin D3 metabolism. FEBS J. 2005; 272:4080–4090. [PubMed: 16098191]

6. Tuckey RC, Li W, Zjawiony JK, Zmijewski MA, Nguyen MN, Sweatman T, Miller D, Slominski A. Pathways products for the metabolism of vitamin D3 by cytochrome P450scc. FEBS J. 2008; 275:2585–2596. [PubMed: 18410379]

7. Slominski AT, Kim TK, Shehabi HZ, Semak I, Tang EK, Nguyenb MN, Benson HA, Korik E, Janjetovic Z, Chen J, Yates CR, Postlethwaite A, Li W, Tuckey RC. In vivo evidence for a novel pathway of vitamin D(3) metabolism initiated by P450scc modified by CYP27B1. FASEB J. 2012; 26:3901–3915. [PubMed: 22683847]

8. Slominski AT, Li W, Kim TK, Semak I, Wang J, Zjawiony JK, Tuckey RC. Novel activities of CYP11A1 and their potential physiological significance. J Steroid Biochem Mol Biol. 2015; 151:25–37. [PubMed: 25448732]

9. Slominski AT, Kim TK, Li W, Yi AK, Postlethwaite A, Tuckey RC. The role of CYP11A1 in the production of vitamin D metabolites and their role in the regulation of epidermal functions. J Steroid Biochem Mol Biol. 2014; 144(Part A):28–39. [PubMed: 24176765]

10. Slominski AT, Kim TK, Li W, Postlethwaite A, Tieu EW, Tang EK, Tuckey RC. Detection of novel CYP11A1-derived secosteroids in the human epidermis and serum and pig adrenal gland. Sci Rep. 2015; 5:14875. [PubMed: 26445902]

11. Slominski AT, Kim TK, Janjetovic Z, Tuckey RC, Bieniek R, Yue J, Li W, Chen J, Nguyen MN, Tang EK, Miller D, Chen TC, Holick M. 20-Hydroxyvitamin D2 is a noncalcemic analog of vitamin D with potent antiproliferative prodifferentiation activities in normal malignant cells. Am J Physiol Cell Phvsiol. 2011; 300:C526–541.

12. Kim TK, Wang J, Janjetovic Z, Chen J, Tuckey RC, Nguyen MN, Tang EK, Miller D, Li W, Slominski AT. Correlation between secosteroid-induced vitamin D receptor activity in melanoma cells computer-modeled receptor binding strength. Mol Cell Endocrinol. 2012; 361:143–152. [PubMed: 22546549]

13. Slominski AT, Kim TK, Takeda Y, Janjetovic Z, Brozyna AA, Skobowiat C, Wang J, Postlethwaite A, Li W, Tuckey RC, Jetten AM. RORalpha ROR gamma are expressed in human skin serve as receptors for endogenously produced noncalcemic 20-hydroxy- and 20,23-dihydroxyvitamin D. FASEB J. 2014; 28:2775–2789. [PubMed: 24668754]

14. Tuckey RC, Li W, Shehabi HZ, Janjetovic Z, Nguyen MN, Kim TK, Chen J, Howell DE, Benson HAE, Sweatman T, Baldisseri DM, Slominski A. Production of 22-hydroxy metabolites of vitamin D-3 by cytochrome P450scc (CYP11A1) and analysis of their biological activities on skin cells. Drug Metab Dispos. 2011; 39:1577–1588. [PubMed: 21677063]

15. Slominski AT, Janjetovic Z, Fuller BE, Zmijewski MA, Tuckey RC, Nguyen MN, Sweatman T, Li W, Zjawiony J, Miller D, Chen TC, Lozanski G, Holick MF. Products of vitamin D3 or 7-dehydrocholesterol metabolism by cytochrome P450scc show anti-leukemia effects, having low or absent calcemic activity. PLoS One. 2010; 5:e9907. [PubMed: 20360850]

16. Slominski AT, Janjetovic Z, Kim TK, Wright AC, Grese LN, Riney SJ, Nguyen MN, Tuckey RC. Novel vitamin D hydroxyderivatives inhibit melanoma growth and show differential effects on normal melanocytes. Anticancer Res. 2012; 32:3733–3742. [PubMed: 22993313]

17. Janjetovic Z, Brozyna AA, Tuckey RC, Kim TK, Nguyen MN, Jozwicki W, Pfeffer SR, Pfeffer LM, Slominski AT. High basal NF-kappaB activity in nonpigmented melanoma cells is associated with an enhanced sensitivity to vitamin D3 derivatives. Br J Cancer. 2011; 105:1874–1884. [PubMed: 22095230]

18. Janjetovic Z, Tuckey RC, Nguyen MN, Thorpe EM Jr, Slominski AT. 20,23-dihydroxyvitamin D3, novel P450scc product, stimulates differentiation and inhibits proliferation and NF-kappaB activity in human keratinocytes. J Cell Phvsiol. 2010; 223:36–48.

19. Janjetovic Z, Zmijewski MA, Tuckey RC, DeLeon DA, Nguyen MN, Pfeffer LM, Slominski AT. 20-Hydroxycholecalciferol, product of vitamin D3 hydroxylation by P450scc, decreases NF-kappaB activity by increasing IkappaB alpha levels in human keratinocytes. PLoS One. 2009; 4:e5988. [PubMed: 19543524]

20. Slominski A, Janjetovic Z, Tuckey RC, Nguyen MN, Bhattacharya KG, Wang J, Li W, Jiao Y, Gu W, Brown M, Postlethwaite AE. 20S-hydroxyvitamin D3, noncalcemic product of CYP11A1 action on vitamin D3, exhibits potent antifibrogenic activity in vivo. J Clin Endocrinol Metab. 2013; 98:E298–303. [PubMed: 23295467]

21. Wang Q, Lin Z, Kim TK, Slominski AT, Miller DD, Li W. Total synthesis of biologically active 20S-hydroxyvitamin D3. Steroids. 2015; 104:153–162. [PubMed: 26433048]

22. Chen J, Wang J, Kim TK, Tieu EW, Tang EKY, Lin Z, Kovacic D, Miller DD, Postlethwaite A, Tuckey RC, Slominski AT, Li W. Novel vitamin D analogs as potential therapeutics: metabolism, toxicity profiling, and antiproliferative activity. Anticancer Res. 2014; 34:2153–2163. [PubMed: 24778017]

23. Xiao M, Wang J, Lin Z, Lu Y, Li Z, White SW, Miller DD, Li W. Design, synthesis and structure-activity relationship studies of novel survivin inhibitors with potent anti-proliferative properties. PLoS One. 2015; 10:e0129807. [PubMed: 26070194]

24. Lin Z, Marepally SR, Ma D, Myers LK, Postlethwaite AE, Tuckey RC, Cheng CY, Kim TK, Yue J, Slominski AT, Miller DD, Li W. Chemical synthesis and biological activities of 20S,24S/R-dihydroxyvitamin D3 epimers and their 1alpha-hydroxyl derivatives. J Med Chem. 2015; 58:7881–7887. [PubMed: 26367019]

25. Li W, Chen J, Janjetovic Z, Kim TK, Sweatman T, Lu Y, Zjawiony J, Tuckey RC, Miller D, Slominski A. Chemical synthesis of 20S-hydroxyvitamin D3, which shows antiproliferative activity. Steroids. 2010; 75:926–935. [PubMed: 20542050]

26. Lu Y, Chen J, Janjetovic Z, Michaels P, Tang EK, Wang J, Tuckey RC, Slominski AT, Li W, Miller DD. Design, synthesis, and biological action of 20R-hydroxyvitamin D3. J Med Chem. 2012; 55:3573–3577. [PubMed: 22404326]

27. Tang EK, Li W, Janjetovic Z, Nguyen MN, Wang Z, Slominski A, Tuckey RC. Purified mouse CYP27B1 can hydroxylate 20,23-dihydroxyvitamin D3, producing 1alpha,20,23-trihydroxyvitamin D3, which has altered biological activity. Drug Metab Dispos. 2010; 38:1553–1559. [PubMed: 20554701]

28. Lin Z, Yang R, Guan Z, Chen A, Li W. Ultra-performance LC separation and quadrupole time-of-flight MS identification of major alkaloids in Plumula Nelumbinis. Phvtochem Anal. 2014; 25:485–494.

29. Pingili AK, Kara M, Khan NS, Estes AM, Lin Z, Li W, Gonzalez FJ, Malik KU. 6beta-hydroxytestosterone, a cytochrome P450 1B1 metabolite of testosterone, contributes to angiotensin II-induced hypertension and its pathogenesis in male mice. Hypertension. 2015; 65:1279–1287. [PubMed: 25870196]

30. Cheng CY, Slominski AT, Tuckey RC. Metabolism of 20-hydroxyvitamin D3 by mouse liver microsomes. J Steroid Biochem Mol Biol. 2014; 144(PartB):286–293. [PubMed: 25138634]

31. Tang EK, Chen J, Janjetovic Z, Tieu EW, Slominski AT, Li W, Tuckey RC. Hydroxylation of CYP11A1-derived products of vitamin D3 metabolism by human and mouse CYP27B1. Drug Metab Dispos. 2013; 41:1112–1124. [PubMed: 23454830]

32. Meyaard L. The inhibitory collagen receptor LAIR-1 (CD305). J Leukocyte Biol. 2008; 83:799–803. [PubMed: 18063695]

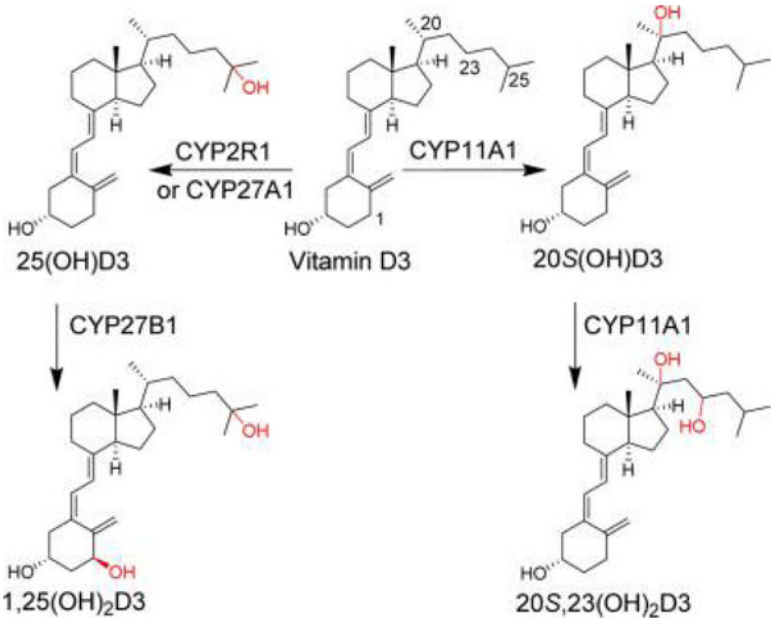

Figure 1.

VD3 is metabolized to 25(OH)D3 and 1,25(OH)$_2$D3 by the classical pathway or to 20*S*(OH)D3 and 20*S*,23(OH)$_2$D3 by CYP11A1.

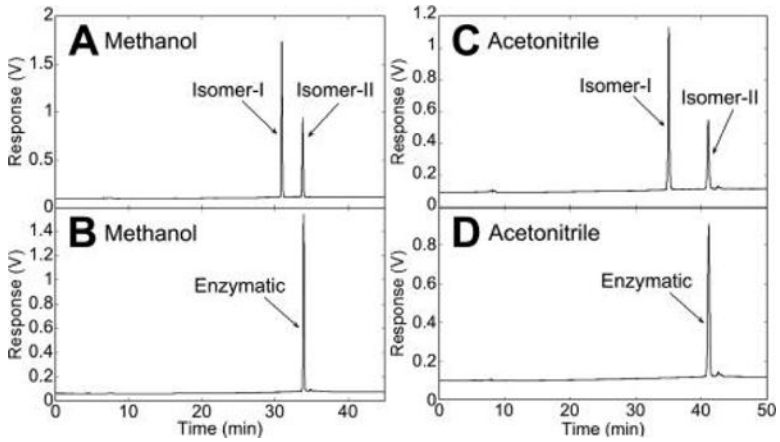

Figure 2.

Comparison of HPLC retention times of 20*S*,23(OH)$_2$D3 isomers produced chemically and enzymatically. Chemically synthesized isomer I (2 nmol) and isomer II (1 nmol) were combined (A,C) and analyzed by HPLC in comparison to 2 nmol enzymatically synthesized 20*S*,23(OH)$_2$D3 (B,D). Isomer II (**17b**) was found to be the enzymatically produced isomer.

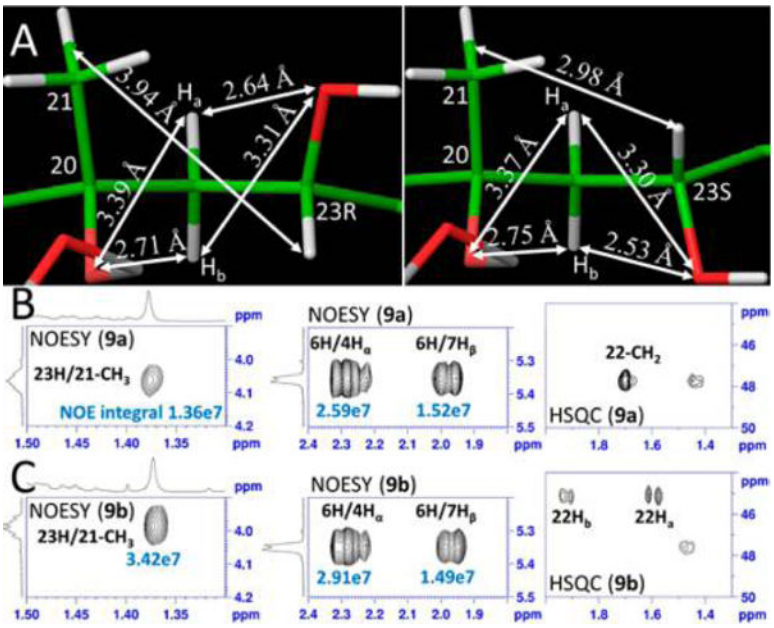

Figure 3.

Molecular models (A) after energy minimization and the 2D NMR for **9a** (23*R*) (B) and **9b** (23*S*) (C). The distance (3.94 Å) between 23H and the centroid of 21-CH_3 in the 23*R*-configuration is longer than that of the 23*S*-configuration based on their NOE peak integrals. The chemical environments for $22H_a$ and $22H_b$ are affected by 23-O and 20-O symmetrically in the 23*R*-configuration, and thus they have similar chemical shifts. In contrast, these two protons are in different environments created by the 23-O and 20-O in 23*S*-configuration and thus have very different chemical shifts.

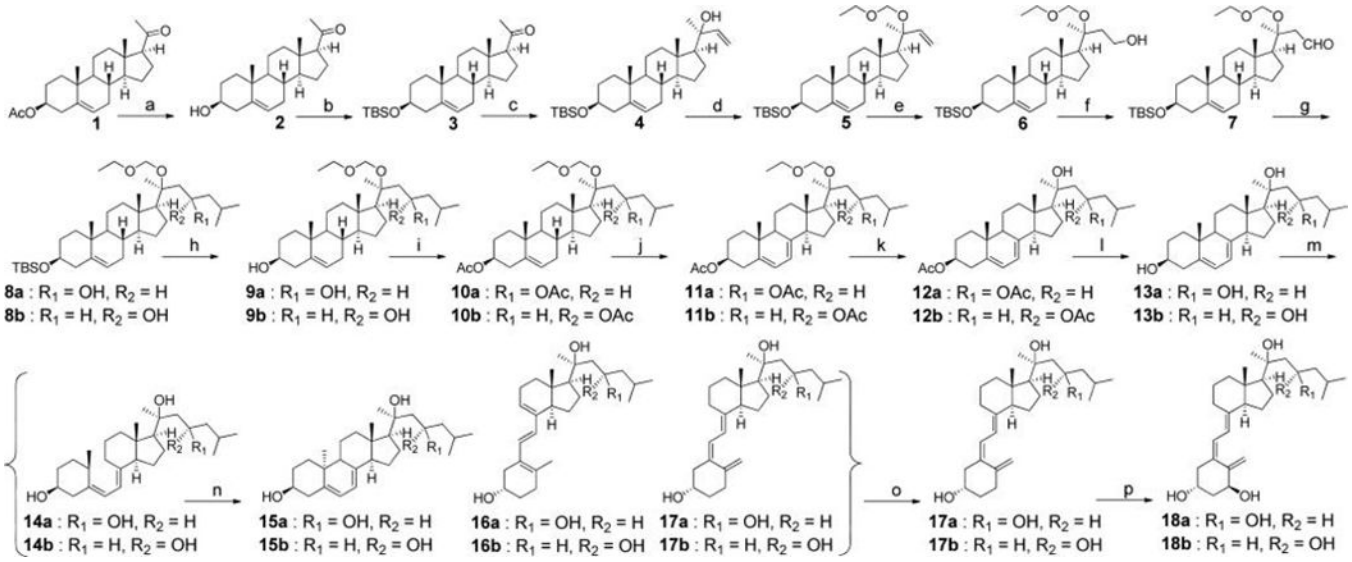

Scheme 1. Synthesis of Compounds 17 and 18[a]

[a]Reagents and conditions: (a) aq KOH, MeOH, rt, 2 h, 94%. (b) TBSCl, imidazole, DMF, rt, overnight, 92%. (c) Vinylmagnesium bromide, THF, 0 °C to rt, overnight, 84%. (d) EOMCl, DIPEA, CH_2Cl_2, rt, overnight, 92%. (e) 9-BBN, THF, 0 °C to rt, 24 h; H_2O, rt, 0.5 h; NaOH, H_2O_2, −20 °C to rt, overnight, 81%. (f) PDC, CH_2Cl_2, rt, 24 h, 96%. (g) Isobutyl bromide, Mg, THF, I_2, 45 °C, 1 h; THF, 0 °C to rt, 6 h, 85%. (h) TBAF, THF, rt, 12 h, 100%. (i) Ac_2O, pyridine, DMAP, 12 h, 94%. (j) Dibromantin, AIBN, benzene:hexane (l:l), reflux 20 min; TBAB, THF, rt, 75 min, then TBAF, rt, 50 min, 39%. (k) Mont. K10, ACN, 0 °C to rt, 12 h, 65% (35% recovered). (l) aq KOH, MeOH, 2 h, 85%. (m) UVB, Et_2O, 15 min. (n) Ethanol, reflux, 3 h. (o) HPLC, ACN:H_2O, 11% (three steps). Overall yield from step (a) to (o) is 1.5%. (p) CYP27B1 enzyme.

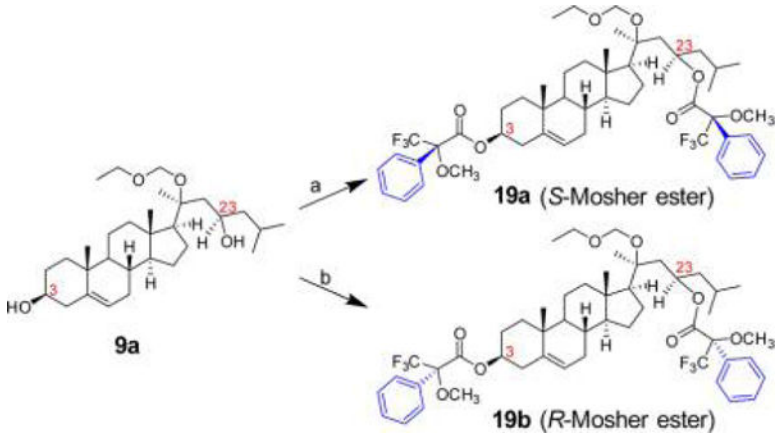

Scheme 2. Synthesis of Mosher Esters 19a and 19b[a]

[a]Reagents and conditions: (a) (*R*)-Mosher acid chloride, Et_3N, DMAP, DCM, rt, overnight, 80%. (b) (*S*)-Mosher acid chloride, Et_3N, DMAP, DCM, rt, overnight, 88%.

Table 1

^{1}H-NMR Chemical Shifts of 9a, *S*- and *R*-Mosher Esters ($\Delta\delta = \delta S - \delta R$)[a]

	^{1}H NMR chemical shift (ppm)					
	C3 of 9a is *S*			C23 of 9a is *R*		
	$2H_\alpha$	$2H_\beta$	4-CH_2	22-CH_2	24H′	24H″
9a	1.84	1.51	2.26	1.68	1.43	1.10
19a (*S*-ester)	1.91	1.61	2.46	1.92	1.63	1.48
19b (*R*-ester)	1.98	1.73	2.36	1.96	1.58	1.44
$\Delta\delta$	−0.07	−0.08	0.10	−0.04	0.05	0.04

[a]The C3-configuration was used as an internal standard. Chemical shifts of Mosher esters were assigned from ^{1}H–^{3}H COSY spectra.

Table 2

Kinetics of the Metabolism of 20*S*,23*R*(OH)$_2$D3 and 17b by CYP27B1[a]

substrate	K_m	k_{cat}	k_{cat}/K_m
20*S*,23*R*(OH)$_2$D3 (**17a**)	2.3 ± 0.8	1.17 ± 0.08	5087
20*S*,23*S*(OH)$_2$D3 (**17b**)	5.2 ± 1.8	2.46 ± 0.22	4731

[a] K_m, 10^{-3} mol/mol phospholipid (PL); k_{cat}, min^{-1}; k_{cat}/K_m, min^{-1} $(mmol/mol\ PL)^{-1}$.

Table 3

Biological Activities of 20*S*,23*R*(OH)$_2$D3, 20*S*,23*S*(OH)$_2$D3 and Their 1α-OH Derivatives Compared to 1,25(OH)$_2$D3 and 22-oxa-1,25(OH)$_2$D3[a]

	VDRE activation (EC50, nM)			
compd	**HaCaT**	**Caco-2**	**Jurkat**	**LAIR1 level (MF, AU)**
vehicle control	NA	NA	NA	766 ± 22
20*S*,23*R*(OH)$_2$D3 (**17a**)	484 ± 28	562 ± 34	653 ± 61	1481 ± 24
20*S*,23*S*(OH)$_2$D3 (**17b**)	NS	NS	NS	1479 ± 98
1α,20*S*,23*R*(OH)$_3$D3 (**18a**)	116.9 ± 0.21	171.7 ± 3.4	30.64 ± 0.39	1478 ± 78
1α,20*S*,23*S*(OH)$_3$D3 (**18b**)	174.8 ± 8.2	241.4 ± 10	203.0 ± 12.9	1480 ± 53
1,25(OH)$_2$D3	249.7 ± 1.8	223.4 ± 0.8	3.936 ± 0.070	1355 ± 28
22-oxa-1,25(OH)$_2$D3	159.7 ± 3.4	144.5 ± 3.0	0.855 ± 0.036	1479 ± 72

[a]NA: not applicable. NS: no significance. MF: mean fluorescence. LAIR1 levels were measured at 100 nM of compound.